atoms

MDPI

Article

Rayleigh and Raman Scattering from Alkali Atoms

Adam Singor [1,*], Dmitry Fursa [1], Keegan McNamara [2] and and Igor Bray [1]

[1] Curtin Institute for Computation and Department of Physics and Astronomy, Curtin University, Perth, WA 6102, Australia; D.Fursa@curtin.edu.au (D.F.); Igor.Bray@curtin.edu.au (I.B.)
[2] Institute for Theoretical Physics, ETH Zurich, 8093 Zürich, Switzerland; mkeegan@student.ethz.ch
* Correspondence: adam.singor@student.curtin.edu.au

Received: 14 August 2020; Accepted: 3 September 2020; Published: 7 September 2020

Abstract: Two computational methods developed recently [McNamara, Fursa, and Bray, Phys. Rev. A **98**, 043435 (2018)] for calculating Rayleigh and Raman scattering cross sections for atomic hydrogen have been extended to quasi one-electron systems. A comprehensive set of cross sections have been obtained for the alkali atoms: lithium, sodium, potassium, rubidium, and cesium. These cross sections are accurate for incident photon energies above and below the ionization threshold, but they are limited to energies below the excitation threshold of core electrons. The effect of spin-orbit interaction, importance of accounting for core polarization, and convergence of the cross sections have been investigated.

Keywords: rayleigh; raman; photon scattering; alkali; complex scaling

1. Introduction

A fully quantum mechanical approach to photon-atom scattering processes has been well understood since the mid 1920's with the development of the Kramers–Heisenberg–Waller (KHW) matrix elements [1,2]. The KHW matrix elements describe photon-atom interactions to second order in perturbation theory. Since then, photon-atom and photon-molecule scattering cross sections have proved to be essential for many applications, such as modelling opacity and radiative transport [3–5], Raman spectroscopy [6], and quantum illumination and radar [7,8]. The main difficulties that arise when calculating KHW matrix elements are related to the inclusion of the contribution from the continuum spectrum of the target and accounting for the pole terms that appear for incident photon energies that are above the ionization threshold.

Historically, the full account of the target spectrum in the calculations of the KHW matrix elements has been limited to atomic hydrogen, where the Green's function and bound-bound and bound-free matrix elements can be evaluated analytically [9,10]. An alternative approach that avoids a direct evaluation of the pole terms and infinite summations over intermediate states was developed by Dalgarno and Lewis [11]. Sadeghpour and Dalgarno [12] applied this technique to the calculation of Rayleigh and Raman scattering cross sections for hydrogen and cesium. For more complex targets, the common approach is to only use a number of low lying bound states assuming contributions from all other states are negligible. Delserieys et al. [13] calculated Rayleigh and Raman scattering from the $3s3p\,^3P_J$ metastable states of magnesium by including a few low-lying intermediate bound states. Drühl [14] considered anti-Stokes Raman scattering on atomic iodine for small incident photon energies, where the infinite summation over intermediate states was approximated while using sum rules. Grunefeld [15] used complex polarizabilties and hyperpolarizabilties to calculate Rayleigh and Raman scattering on various targets, including lithium and sodium.

Recently, we have developed two computational methods for calculating Rayleigh and Raman scattering on hydrogen-like atoms that are valid for incident photon energies above and below

the ionization threshold [16]. The first method involves the direct numerical calculation of KHW matrix elements and utilises principal value integration to deal with pole terms. The second method implements a finite-L^2 expansion of the target and deals with pole terms by using a complex scaling technique that has been widely used to study resonances in atoms and molecules [17–19]. Here these techniques are extended to quasi one-electron atoms and applied to the calculation of Rayleigh and Raman scattering cross sections for alkali atoms: lithium, sodium, potassium, rubidium, and cesium. In the next section, we give a brief formulation of photon scattering and discuss the target structure model for the alkali atoms. In Section 3, we present the generalization of the computational techniques to quasi one-electron atoms. In Section 4, the convergence of the cross sections is demonstrated, the effect of spin-orbit interaction is discussed, and the cross sections for a number of transitions are presented and compared with available previous calculations. Conclusions and future directions are formulated in Section 5. We use atomic units in the paper, unless stated otherwise.

2. Theory

2.1. Photon-Atom Scattering

To second order in perturbation theory, the differential cross section for photon scattering from an initial state $|i\rangle \equiv |\gamma J\rangle$ to a final state $|f\rangle \equiv |\gamma' J'\rangle$, where J is the total angular momentum and γ is all other quantum numbers, is given by

$$\frac{\mathrm{d}\sigma_{fi}}{\mathrm{d}\Omega} = r_0^2 \frac{\omega'}{\omega} \left| M_{fi} \right|^2 . \tag{1}$$

Here, $r_0 = \frac{e^2}{4\pi\epsilon_0 m_e c^2} \approx 2.82 \times 10^{-15}$ m is the classical electron radius and ω and ω' are the incident and outgoing photon energies, respectively. M_{fi} is the KHW matrix element [1,2,20],

$$\begin{aligned} M_{fi} = {} & \boldsymbol{\epsilon} \cdot \boldsymbol{\epsilon}'^{*} \, \langle f | e^{i(\boldsymbol{k}-\boldsymbol{k}')\cdot \boldsymbol{r}} | i \rangle \\ & - \sum\!\!\!\!\!\!\int_t \left[\frac{\langle f | e^{-i\boldsymbol{k}'\cdot\boldsymbol{r}} (\boldsymbol{\epsilon}'^{*} \cdot \boldsymbol{p}) | t \rangle \langle t | e^{i\boldsymbol{k}\cdot\boldsymbol{r}} (\boldsymbol{\epsilon} \cdot \boldsymbol{p}) | i \rangle}{E_t - E_i - \omega - i0} + \frac{\langle f | e^{i\boldsymbol{k}\cdot\boldsymbol{r}} (\boldsymbol{\epsilon} \cdot \boldsymbol{p}) | t \rangle \langle t | e^{-i\boldsymbol{k}'\cdot\boldsymbol{r}} (\boldsymbol{\epsilon}'^{*} \cdot \boldsymbol{p}) | i \rangle}{E_t - E_i + \omega'} \right] , \end{aligned} \tag{2}$$

where E_t is the energy of the state $|t\rangle$, $\boldsymbol{\epsilon}$ ($\boldsymbol{\epsilon}'$) and $\boldsymbol{k}$ ($\boldsymbol{k}'$) are the polarization and momenta of the incident (outgoing) photon. The summation in Equation (2) is over all intermediate bound states and an integral over the continuum. The outgoing photon also satisfies energy conservation $\omega + E_i = E_f + \omega'$. In the long wavelength approximation, that is valid for the relatively low photon energies that are considered in this paper, the KHW matrix elements can be written as,

$$M_{fi} = \omega\omega' \sum\!\!\!\!\!\!\int_t \left[\frac{\langle f | (\boldsymbol{\epsilon}'^{*} \cdot \boldsymbol{r}) | t \rangle \langle t | (\boldsymbol{\epsilon} \cdot \boldsymbol{r}) | i \rangle}{E_t - E_i - \omega - i0} + \frac{\langle f | (\boldsymbol{\epsilon} \cdot \boldsymbol{r}) | t \rangle \langle t | (\boldsymbol{\epsilon}'^{*} \cdot \boldsymbol{r}) | i \rangle}{E_t - E_i + \omega'} \right] . \tag{3}$$

For nonoriented systems, the scattering matrix can be written as a sum of irreducible tensor components [21] and the differential cross section is

$$\begin{aligned} \frac{\mathrm{d}\sigma_{\gamma' J' \gamma J}}{\mathrm{d}\Omega} = r_0^2 \frac{\omega\omega'^3}{3(2J+1)} \Bigg[& \left| A^{(0)}_{\gamma' J' \gamma J} \right|^2 \left| \boldsymbol{\epsilon}'^{*} \cdot \boldsymbol{\epsilon} \right|^2 + \frac{3}{2} \left| A^{(1)}_{\gamma' J' \gamma J} \right|^2 \left(1 - \left| \boldsymbol{\epsilon}' \cdot \boldsymbol{\epsilon} \right|^2 \right) \\ & + \frac{3}{2} \left| A^{(2)}_{\gamma' J' \gamma J} \right|^2 \left(1 + \left| \boldsymbol{\epsilon}' \cdot \boldsymbol{\epsilon} \right|^2 - \frac{2}{3} \left| \boldsymbol{\epsilon}'^{*} \cdot \boldsymbol{\epsilon} \right|^2 \right) \Bigg] , \end{aligned} \tag{4}$$

where the tensor expansion coefficients are

$$A^{(\kappa)}_{\gamma' J' \gamma J} = (-1)^{J+J'+\kappa} \sum_t \begin{Bmatrix} J & J' & \kappa \\ 1 & 1 & J_t \end{Bmatrix} \langle \gamma' J' || r || \gamma_t J_t \rangle \langle \gamma_t J_t || r || \gamma J \rangle \times \left[\frac{1}{E_{\gamma_t J_t} - E_{\gamma J} - \omega + i0} + \frac{(-1)^\kappa}{E_{\gamma_t J_t} - E_{\gamma J} + \omega'} \right]. \quad (5)$$

After summing over the final polarizations, averaging over initial polarizations and integration over all solid angles, the total integrated cross section for Rayleigh and Raman scattering in the length gauge is

$$\sigma_{\gamma' J' \gamma J} = \sigma_T \frac{\omega \omega'^3}{3(2J+1)} \sum_{\kappa=0}^{2} (2\kappa + 1) \left| A^{(\kappa)}_{\gamma' J' \gamma J} \right|^2, \quad (6)$$

where $\sigma_T = 8\pi r_0^2/3 \approx 6.652 \times 10^{-29}$ m^2 is the Thompson cross section.

The equivalent expressions with the velocity form of the dipole operator are given in [16]. We consider scattering with and without the inclusion of the spin-orbit interaction for the calculation of the target wave functions. The above formulation is valid for both cases if the total angular momentum J is understood to be the orbital angular momentum L in the non-relativistic case $|nLS\rangle$. If fine structure transitions are not of interest the combined cross sections can be found using

$$\sigma_{\gamma' L' \gamma L} = \frac{\sum_{J' J} (2J+1)\, \sigma_{\gamma' J' \gamma J}}{(2L+1)(2S+1)}. \quad (7)$$

Photoionization cross sections can be calculated in this formalism using

$$\sigma^I_{\gamma J} = \sigma_T \frac{3}{2} \frac{c^3 \omega}{\sqrt{3(2J+1)}} \mathrm{Im} \left\{ A^{(0)*}_{\gamma J \gamma J} \right\}. \quad (8)$$

2.2. Quasi One-Electron Atomic Structure

In this paper, the alkali metal atoms are described by a model of a single electron in a central local potential produced by frozen core electrons. The l-dependent potential can be written in the following form,

$$V^{(l)}(r) = V_\mathrm{d}(r) + V_\mathrm{e}^{(l)}(r) + V_\mathrm{p}^{(l)}(r). \quad (9)$$

Here, the direct term is

$$V_\mathrm{d}(r) = -\frac{Z}{r} + \sum_{n_c l_c} (2l_c + 1) \int_0^\infty \mathrm{d}r' \, \frac{\phi^2_{n_c l_c}(r')}{\max(r, r')}, \quad (10)$$

where the $\phi_{n_c l_c}(r)$ are core orbitals that are given by Clementi and Roetti [22] for $Z < 55$ and McLean and McLean [23] for $55 \leq Z \leq 92$. The equivalent local exchange term that is introduced by Furness and McCarthy [24] is

$$V_\mathrm{e}^{(l)}(r) = -\frac{\alpha^{(l)}_\mathrm{exch}}{2} \left\{ \left[\left(E - V_\mathrm{d}(r) \right)^2 + 4\pi\rho(r) \right]^{1/2} - \left(E - V_\mathrm{d}(r) \right) \right\}, \quad (11)$$

where

$$\rho(r) = \sum_{n_c l_c} (2l_c + 1) \frac{\phi^2_{n_c l_c}(r)}{4\pi r^2}, \quad (12)$$

and $\alpha_{\rm exch}^{(l)}$ is a parameter that is chosen, for each orbital angular momentum l, in order to ensure the local exchange potential is equivalent to its non-local counterpart. We set $E = 0$ to ensure orthogonal orbitals [25]. The dipole polarization potential [26] is

$$V_{\rm p}^{(l)}(r) = -\frac{\alpha_D}{2r^4}\left[1 - \exp\left(-\left(\frac{r}{r_c^{(l)}}\right)^6\right)\right] \tag{13}$$

where α_D is the static dipole polarizability of the core ion and $r_c^{(l)}$ is a cut-off radius that is chosen for each l by fitting to the experimental energy levels. Quadrupole and octopole polarizability potential terms were also considered, but were found to be negligible for our calculations.

Spin–orbit interaction was included by adding the following term to the potential in Equation (9),

$$V_{lsj}(r) = \alpha_{lsj}^{(l)} \frac{j(j+1) - l(l+1) - \frac{3}{4}}{4c^2 r} \frac{{\rm d}V^{(l)}}{{\rm d}r}, \tag{14}$$

where $\alpha_{lsj}^{(l)}$ is a parameter that was chosen for each l to ensure that the splitting of the lowest level above the core matched the experimental values.

To account for core polarization more accurately, we have also performed calculations using the modified length form of the dipole operator [27,28]

$$r \to r\left(1 - \frac{\alpha_D}{r^3}\left[1 - \exp\left(-\left(\frac{r}{r_c^{(l)}}\right)^6\right)\right]^{1/2}\right). \tag{15}$$

Table 1 provides the parameters used to construct the models potentials for each atom. We choose to use an l-dependent potential as it yields more accurate energy levels though it leads to a small discrepancy between cross sections calculated using the length and velocity forms of the dipole operator.

Table 1. Local central model potential parameters for alkali atoms. The '−' indicates that this part of the potential is found to be insignificant. The static dipole polarizability of the ionic cores is from [29].

Parameter	Lithium	Sodium	Potassium	Rubidium	Cesium
α_D	0.194	1.001	5.515	9.143	15.805
$\alpha_{\rm exch}^{(0)}$	1.132	1.043	0.617	1.142	0.974
$\alpha_{\rm exch}^{(1)}$	0.766	1.143	0.582	1.226	1.049
$\alpha_{\rm exch}^{(2)}$	0.405	0.716	0.775	1.108	1.058
$\alpha_{\rm exch}^{(3)}$	–	0.399	0.461	0.591	0.649
$r_c^{(0)}$	1.387	1.383	2.072	2.079	2.116
$r_c^{(1)}$	1.274	1.589	2.133	2.416	2.637
$r_c^{(2)}$	2.316	1.727	2.444	2.975	3.613
$r_c^{(3)}$	–	4.043	2.842	2.866	2.984
$\alpha_{lsj}^{(1)}$	0.40	0.83	0.74	0.84	0.82
$\alpha_{lsj}^{(2)}$	0.50	0.81	0.60	–	0.41
$\alpha_{lsj}^{(3)}$	–	–	–	2.00	6.50

3. Calculation Methods

In this section, we summarise the two computational methods used and the changes from their previous implementation for photon scattering on atomic hydrogen [16]. Section 3.1 describes a direct approach for calculating the pole terms in the tensor expansion coefficients, while, in Section 3.2, we describe an approach that utilises analytic continuation into the complex plane to avoid dealing with the pole terms associated with incident photon energies above the ionisation threshold. For both methods, we find it necessary to include a complete set of intermediate states, which means including core orbitals, though typically in electron/positrons scattering only states above the core are included. The calculated cross sections are only valid for incident photon energies below the excitation threshold for the core electrons, given the limitations of the frozen-core model used in this work for the alkali atoms.

3.1. Principal Value Approach

The principal value (PV) method calculates the tensor expansion coefficients directly. The sum presented in Equation (5) is broken into a sum over bound states and a Cauchy principal value integral over the continuum with an imaginary pole term,

$$\begin{aligned} A^{(\kappa)}_{n'l'j'nlj} = (-1)^{j+j'+\kappa} \sum_t \begin{Bmatrix} j & j' & \kappa \\ 1 & 1 & j_t \end{Bmatrix} \Bigg(& \sum_{n_t=l_t+1}^{N_b} \langle n'l'j' || r || n_t l_t j_t \rangle \langle n_t l_t j_t || r || nlj \rangle \\ & \times \left[\frac{1}{E_{n_t l_t j_t} - E_{nlj} - \omega} + \frac{(-1)^\kappa}{E_{n_t l_t j_t} - E_{nlj} + \omega'} \right] + \mathcal{P} \int \mathrm{d}E \, \frac{\langle n'l'j' || r || El_t j_t \rangle \langle El_t j_t || r || nlj \rangle}{E - E_{nlj} - \omega} \\ & + i\pi \, \langle n'l'j' || r || (E_{nlj} + \omega) l_t j_t \rangle \langle (E_{nlj} + \omega) l_t j_t || r || nlj \rangle \\ & + (-1)^\kappa \int \mathrm{d}E \, \frac{\langle n'l'j' || r || El_t j_t \rangle \langle El_t j_t || r || nlj \rangle}{E - E_{nlj} + \omega'} \Bigg). \end{aligned} \tag{16}$$

Previously, for hydrogen [16], this was done while using exact bound and continuum eigenstates. For the alkali atoms, box-based bound states [30] and distorted Coulomb continuum waves are used. If $E_{nlj} + \omega > 0$ the principal value integral is calculated using a Gaussian quadrature method developed by Bray and Stelbovics [31]; however, when $E_{nlj} + \omega < 0$ the PV integral reduces to a regular integral and the imaginary pole term in Equation (16) can be ignored. Convergence is achieved by increasing the number of intermediate bound states and quadrature points. This method is relatively computationally inefficient, as the quadrature chosen depends on the energy of the initial state and the incident photon energy. Thus, a new set of quadrature points and continuum waves must be calculated for each incident photon energy above the ionisation threshold.

The spin-orbit term, Equation (14), introduces a $(1/r^3)$ singularity at the origin. This causes difficulties when calculating continuum $l > 0$ states. Therefore, the PV method is used to calculate cross sections without spin–orbit interaction. Given its relative inefficiency, it is used as an independent verification of the corresponding complex scaling (CS) method results at selected photon energies.

3.2. Complex Scaling Method

The CS method is based on the work of Rescigno and McKoy [19], who used the method to calculate photoionization cross sections for atomic hydrogen. For hydrogen, we start by analytically continuing the radial coordinates of the Hamiltonian by rotating them into the complex plane, $r \to r\theta$, where $\theta = e^{i\varphi}$ and $0 < \varphi < \pi/2$, thus the complex scaling Hamiltonian is defined as $H_\theta \equiv H(\boldsymbol{r}\theta)$. This is only possible when the potential is known analytically. For the alkali atoms, we use a numerical potential and instead apply the conjugate complex scaling factor to the radial coordinates of the basis

functions, i.e., $r \to r/\theta = r\theta^*$. This is equivalent to applying the complex scaling to the potential, as can be seen from the integral

$$\int_0^\infty \mathrm{d}r\, \xi_{k'l}(r) V(r\theta) \xi_{kl}(r) = \theta^* \int_0^\infty \mathrm{d}r\, \xi_{k'l}(r\theta^*) V(r) \xi_{kl}(r\theta^*). \tag{17}$$

For simplicity, in what follows we will refer to the rotated Hamiltonian while meaning the complex scaled Hamiltonian matrix elements, Equation (17). With this modification, the CS procedure is identical to the case for hydrogen.

We diagonalize both the rotated and non-rotated Hamiltonians in a finite-L^2 basis. We use the radial Laguerre functions that are commonly used in the convergent close-coupling formalism [32,33],

$$\xi_{kl}(r) = \sqrt{\frac{\alpha_l (k-1)!}{(k+l)(k+2l)!}} (2\alpha_l r)^{l+1}\, e^{-\alpha_l r}\, L_{k-1}^{2l+1}(2\alpha_l r), \tag{18}$$

where L_n^m are the associated Laguerre polynomials. The discrete eigenvalues of such a Hamiltonian remain unrotated, while the continuous eigenvalues are rotated in the complex plane by -2φ, as can be seen in Figure 1.

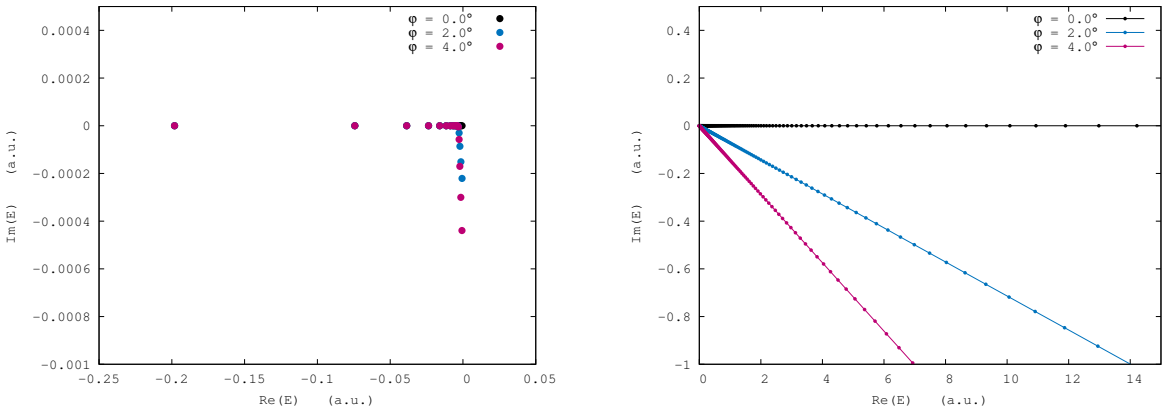

Figure 1. Bound state and discretized continuum energies ($l = 0$) of the lithium atom for different rotation angles. Bound state energies that have a non-zero imaginary component are pseudostates, the larger the imaginary component of the energy the further the bound pseudostate is from an eigenstate.

From the diagonalization procedure, we obtain complex scaled pseudostates of the non-rotated Hamiltonian

$$\psi_{nljm}(\boldsymbol{r}\theta) = \frac{1}{r\theta} u_{nlj}(r\theta)\, Y_j^m(\hat{\boldsymbol{r}}), \quad u_{nlj}(r\theta) = \sum_k a_{njk}\, \xi_{kl}(r\theta) \tag{19}$$

where a_{njk} are real expansion coefficients. Similarly, we generate pseudostates of the rotated Hamiltonian

$$\chi^\theta_{nljm}(\boldsymbol{r}) = \frac{1}{r} v^\theta_{nlj}(r)\, Y_j^m(\hat{\boldsymbol{r}}), \quad v^\theta_{nlj}(r) = \sum_k b_{njk}\, \xi_{kl}(r) \tag{20}$$

where b_{njk} are complex expansion coefficients. The pseudostates of the rotated Hamiltonian satisfy

$$\left(\chi^\theta_{n'l'j'm'} \middle| H_\theta \middle| \chi^\theta_{nljm}\right)_\theta = W_{nljm} \left(\chi^\theta_{n'l'j'm'} \middle| \chi^\theta_{nljm}\right)_\theta. \tag{21}$$

Here, we have used the c norm defined by Moiseyev et al. [34]

$$\left(\chi^{\theta}_{n'l'j'm'}\middle|\chi^{\theta}_{nljm}\right)_{\theta} = \int \mathrm{d}\boldsymbol{r}\ \chi^{\theta\dagger}_{n'l'j'm'}(\boldsymbol{r})\chi^{\theta}_{nljm}(\boldsymbol{r}), \tag{22}$$

where the dagger indicates the conjugation of the angular part only. The tensor expansion coefficients can be written as

$$A^{(\kappa)}_{n'l'j'nlj} = \theta(-1)^{j+j'+\kappa}\sum_t \begin{Bmatrix} j & j' & \kappa \\ 1 & 1 & j_t \end{Bmatrix} \left(\psi_{n'l'j'}\middle|\middle|r\theta\middle|\middle|\chi^{\theta}_{n_tl_tj_t}\right)_{\theta}\left(\psi_{nlj}\middle|\middle|r\theta\middle|\middle|\chi^{\theta}_{n_tl_tj_t}\right)_{\theta} \times \left[\frac{1}{W_{n_tl_tj_t} - E_{nlj} - \omega} + \frac{(-1)^{\kappa}}{W_{n_tl_tj_t} - E_{nlj} + \omega'}\right], \tag{23}$$

and the reduced dipole matrix elements are

$$\left(\psi_{n'l'j'}\middle|\middle|r\theta\middle|\middle|\chi^{\theta}_{nlj}\right)_{\theta} = (-1)^{j+l'+l+s}\sqrt{(2j+1)(2j'+1)(2l'+1)(2l+1)}\begin{Bmatrix} l & s & j \\ j' & 1 & l' \end{Bmatrix} \times \begin{pmatrix} l & 1 & l' \\ 0 & 0 & 0 \end{pmatrix}\int_0^{\infty}\mathrm{d}r\, u_{n'l'j'}(r\theta)\, r\theta\, v^{\theta}_{nlj}(r). \tag{24}$$

Rayleigh and Raman scattering cross sections can then be calculated while using Equation (6). Convergence is achieved by increasing the basis size.

4. Results

In this section, we discuss the agreement of the cross sections calculated using the PV and CS methods, the length (L) and velocity (V) gauges, the effect of using the modified length (M) form of the dipole operator, the effect of accounting for relativistic effects with the spin-orbit term, and illustrate the convergence of the cross sections with increased number of the intermediate bound states and account of continuum. Subsequently, we present a representative set of integrated Rayleigh and Raman cross sections as a function of incident photon energy for each atom. All of the cross sections presented in this paper are in units of the Thompson cross section.

For calculations using the CS method, we use $N_l = 200 - l$ radial Laguerre basis functions, where the exponential fall-off was chosen, such that an accurate initial and final state were calculated in addition to a large number of bound intermediate states and a high density of near threshold continuum states. The exponential fall-off corresponding to the initial and final state was chosen to be $\alpha_l = 1.5$ for lithium and it was increased in steps of 0.5 up to a maximum of $\alpha_l = 3.5$ for cesium, otherwise for the intermediate states an exponential fall-off of $\alpha_l = 0.5$ was used. We also chose to use a rotation angle of 2°. For calculations using the PV method, 25 bound intermediate states and 110 continuum states were sufficient for achieving convergence and produce an accurate resonance profile.

The length and velocity gauge cross sections should be identical for a central local potential. However, the use of an l-dependent model potential leads to a small difference between the length and velocity gauge results, as illustrated in Figure 2 for Rayleigh and Raman scattering on the ground state of cesium. We have verified that, for all presented transitions, if an l-independent potential is used, then the velocity gauge cross sections are practically identical to the length gauge cross sections. Similarly, the results produced with the PV and CS techniques agree well and, in what follows, we only present the results of the CS method that have been verified using the results of PV method calculations.

We investigated the effect of the different forms of the dipole operator, the length, velocity, and modified length forms Equation (15). This is illustrated in Figure 2 for cesium. As cesium has the largest core polarizability α_D in comparison to other alkali atoms, see Table 1, this should lead to the largest effect among all alkali atoms, however we found only minor differences in most cases.

A substantial effect is only found for Raman scattering cross sections above the ionization threshold for scattering between s states, as shown in Figure 2 for the $6s \rightarrow 7s$ transition. In this case, the results calculated using the modified length form of the dipole operator are significantly smaller. The effect of using the modified form of the dipole operator for scattering (Rayleigh and Raman) on excited states and for lighter alkali atoms is found to be small.

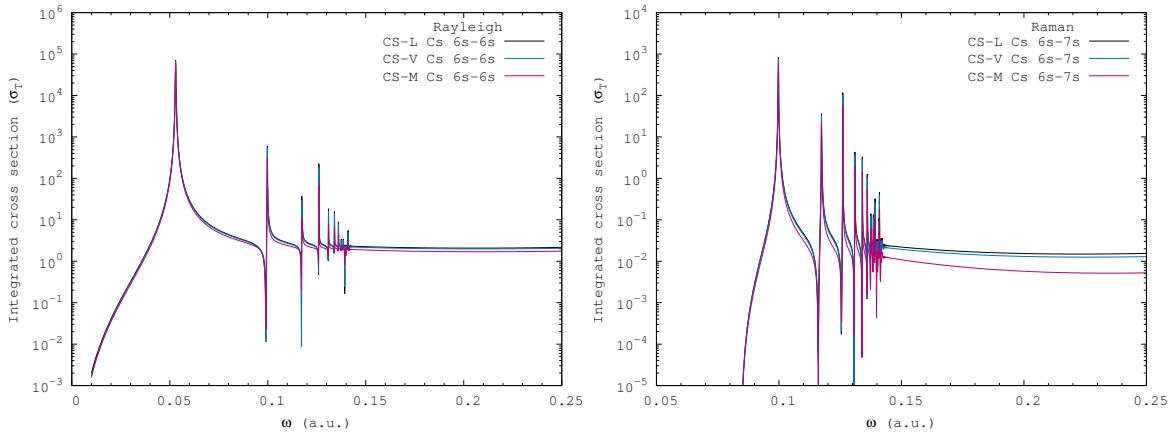

Figure 2. Rayleigh and Raman scattering cross sections for the ground state of cesium calculated using the complex scaling (CS) method. We compare cross sections for different forms of the dipole operator, these being the length (L) gauge, velocity (V) gauge, and modified length (M) defined by Equation (15). The difference between the length and velocity gauge cross sections is due to the use of an l-dependent potential.

The effect of spin-orbit interactions for the CS method is illustrated by considering Rayleigh and Raman scattering on the ground state of atomic cesium, as shown in Figure 3. The cesium atom is the heaviest of the considered atoms with the strongest spin-orbit interaction. Consequently, the largest effect is expected among all of the considered alkali atoms. The fine structure splitting of the low-lying target states leads to corresponding splitting of the peaks in cross sections. For lighter atoms, the fine structure splitting becomes smaller and cross sections become the same as for the non-relativistic approach.

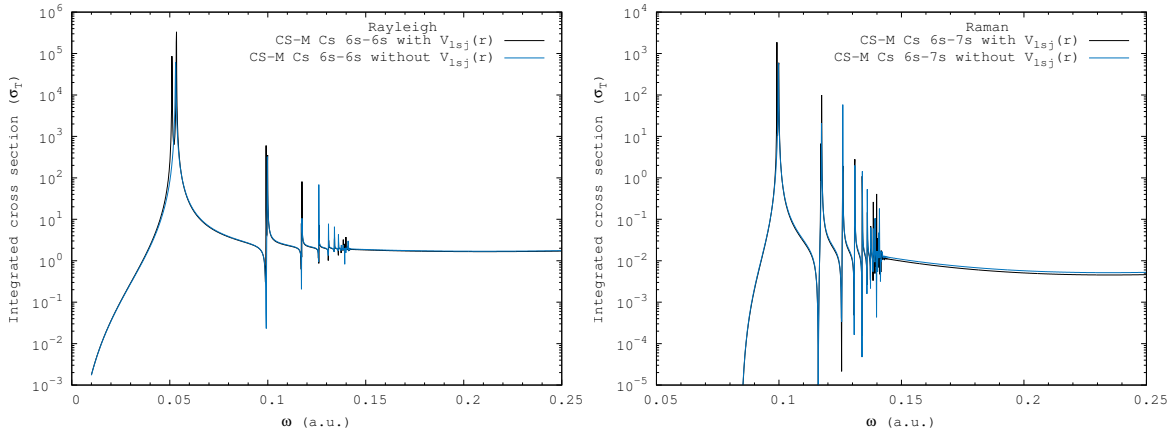

Figure 3. Rayleigh and Raman scattering cross sections for the ground state of cesium with and without spin-orbit interaction. These cross sections were calculated with the CS method using the modified length form of the dipole operator.

The convergence of the cross sections for the CS method using the modified length form of the dipole operator with respect to inclusion of an increased number of bound states and the target continuum is illustrated in Figure 4 for atomic lithium. These results are sufficiently similar to all

other alkali atoms. Below the ionization threshold the cross sections converge after the inclusion of the first few intermediate bound states. The inclusion of more bound states only increases the density of resonances just below the ionisation threshold. Above the ionisation threshold, the inclusion of intermediate continuum states is relatively insignificant for Rayleigh scattering on the ground state, but it has a significant contribution to cross sections for Rayleigh scattering on excited states and Raman scattering. In general, the inclusion of intermediate continuum states and more intermediate bound states becomes more important for scattering from and to higher energy states.

Resonance peaks in the cross sections occurs when the term in the denominators of Equation (2) go through 0. The emission-then-absorption term is resonant when $E_t - E_i + \omega' = 0$, which is, when the incident photon energy is the same as the energy difference between the final state and any intermediate state. The absorption-then-emission term is resonant when $E_t - E_i - \omega = 0$, which is, when the incident photon energy is the same as the energy difference between the initial state and any intermediate state. If $|t\rangle$ is a continuum state, then contour integration is used to avoid any unphysical results. McNamara et al. [16] presented a more detailed discussion of the resonance behaviour. For Raman scattering, intermediate states with an energy between the initial and final state energies are not accessible via the absorption and emission of a single photon. This explains why, in Figure 4, there is no resonance peak that corresponds to the $2p$ or $3p$ state in the lithium $2s \rightarrow 3d$ cross section. The emission followed by absorption of a photon can lead to resonances above the ionisation threshold, as seen in the $3p \rightarrow 3p$ Rayleigh scattering cross section. This is clearly shown by the $2s$ resonance.

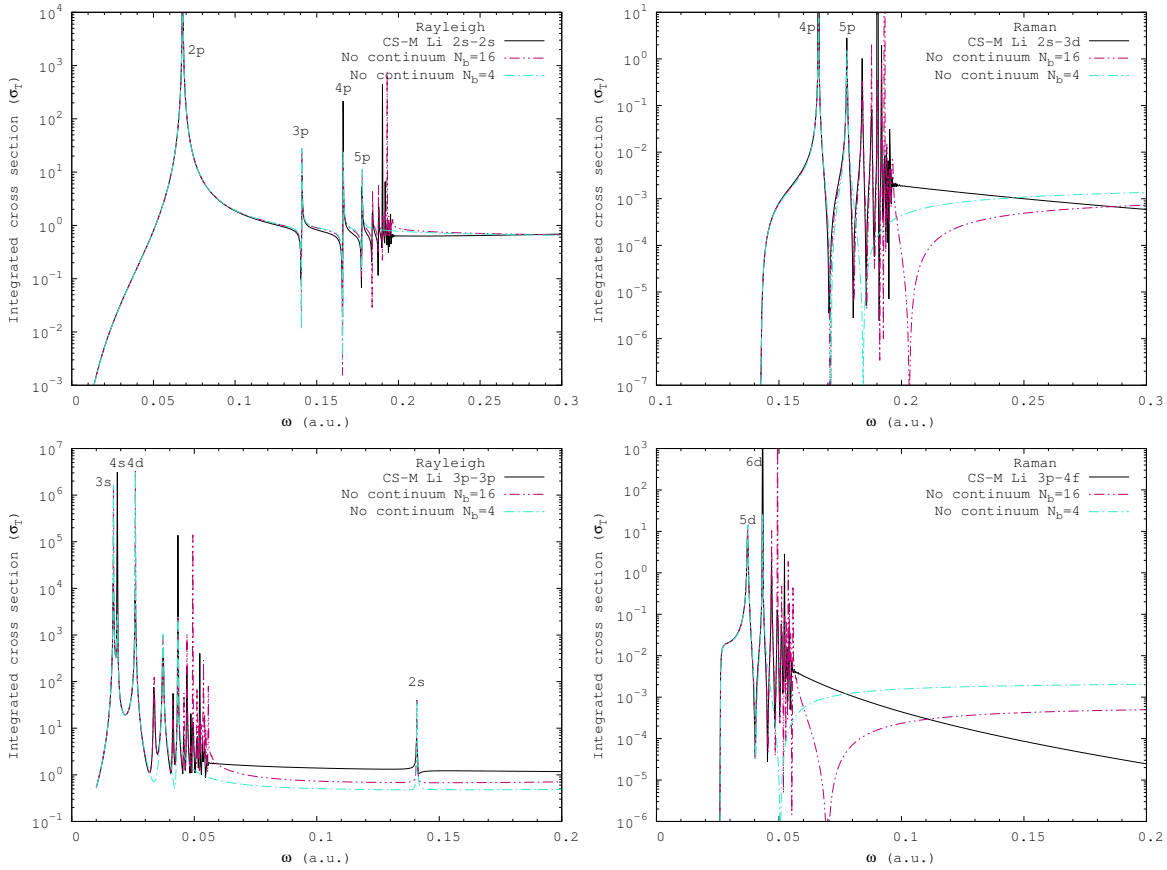

Figure 4. Rayleigh and Raman cross sections for scattering on lithium with increasing number of bound intermediate states and accounting for the target continuum. Cross sections were calculated using the modified length form of the dipole operator and the spin-orbit interaction was neglected. N_b indicates the number of included intermediate bound states.

All of the cross sections presented in the remainder of the paper were calculated with the CS method while using the modified length form of the dipole operator. These calculations were performed using both bound and continuum intermediate states with the number of states increased until convergence was achieved and include spin-orbit interaction. In Figures 5–9, we present a representative set of cross sections. It consists of Rayleigh scattering on the ground state, Raman scattering on the ground state to the first excited d state, Rayleigh scattering on the first excited p state, and Raman scattering on the first excited p state to the first excited f state for each alkali atom from lithium to cesium. Cross sections for combined fine structure levels were found using Equation (7) for lithium, sodium, potassium, and rubidium. For cesium, we present the fine structure resolved cross sections to illustrate the relativistic effects for various transitions. Cross sections were calculated for incident photon energies below a maximum value that is shown in Table 2 for each alkali atom. For incident photon energies greater than this, the cross section is affected by resonances that correspond to the excitation of core electrons. The complete set of cross sections contains Rayleigh cross sections for scattering on the first 10 states with $l \leq 2$ and for each of these states Raman scattering to the first 7 allowed states with $l \leq 3$. These have been calculated for both combined and resolved fine structure levels and will be made available elsewhere.

Table 2. Maximum incident photon energy considered for each alkali atom.

	Lithium	**Sodium**	**Potassium**	**Rubidium**	**Cesium**
$\omega_{\max}$ (a.u.)	1.50	0.65	0.30	0.28	0.25

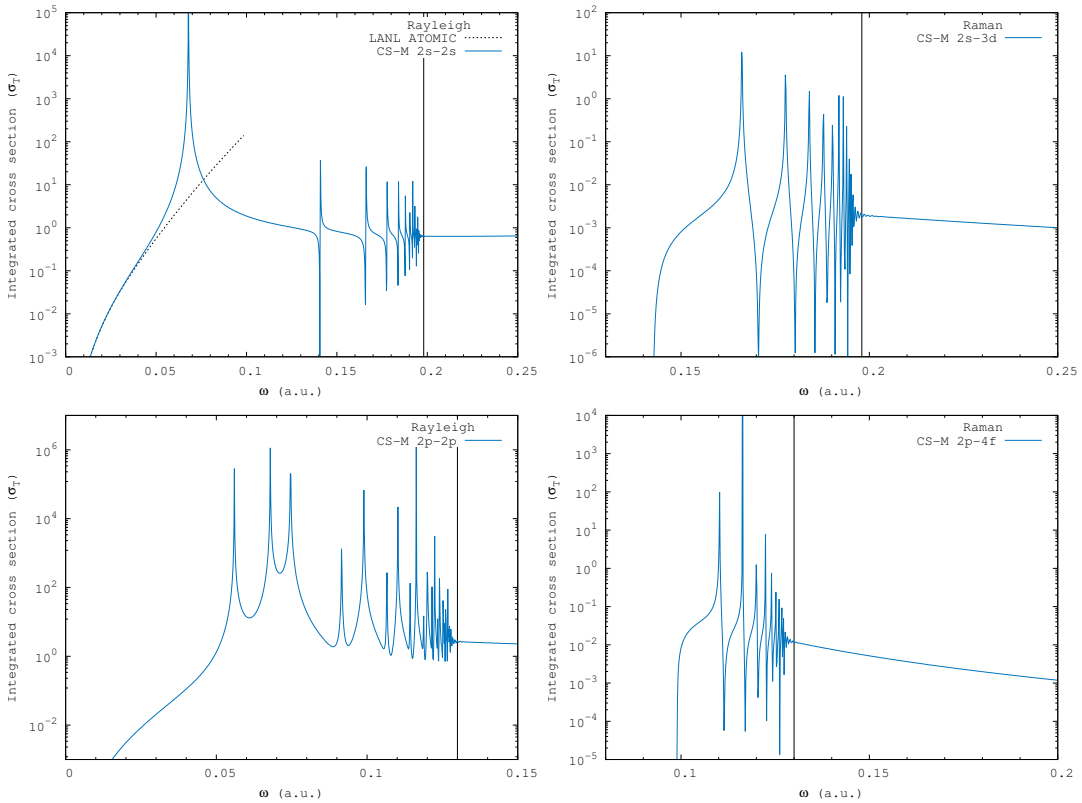

Figure 5. Cross sections for Rayleigh and Raman scattering on ground and excited states of lithium for fine structure combined levels. The 'CS-M' denotes cross sections calculated using the modified length form of the dipole operator in the CS method. The vertical line indicates the ionization threshold. The low energy approximation for the ground state Rayleigh cross sections used in the Los Alamos National Lab (LANL) ATOMIC code [5] is also presented.

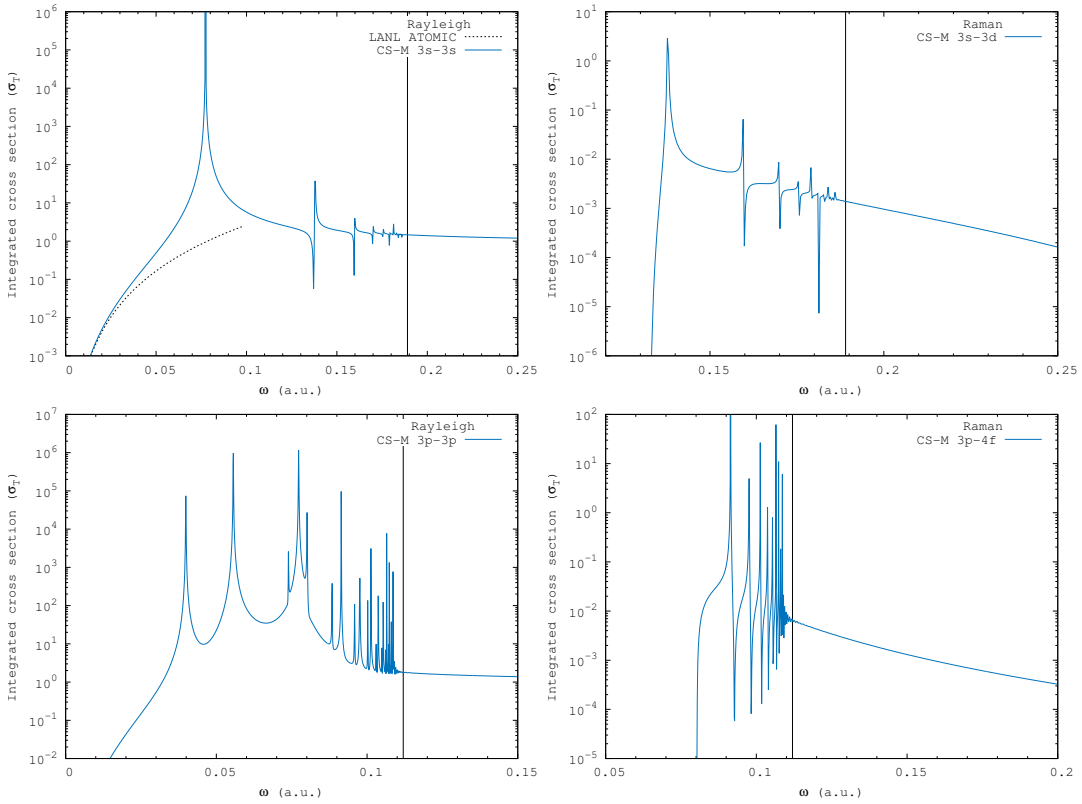

Figure 6. Same as Figure 5 but for sodium.

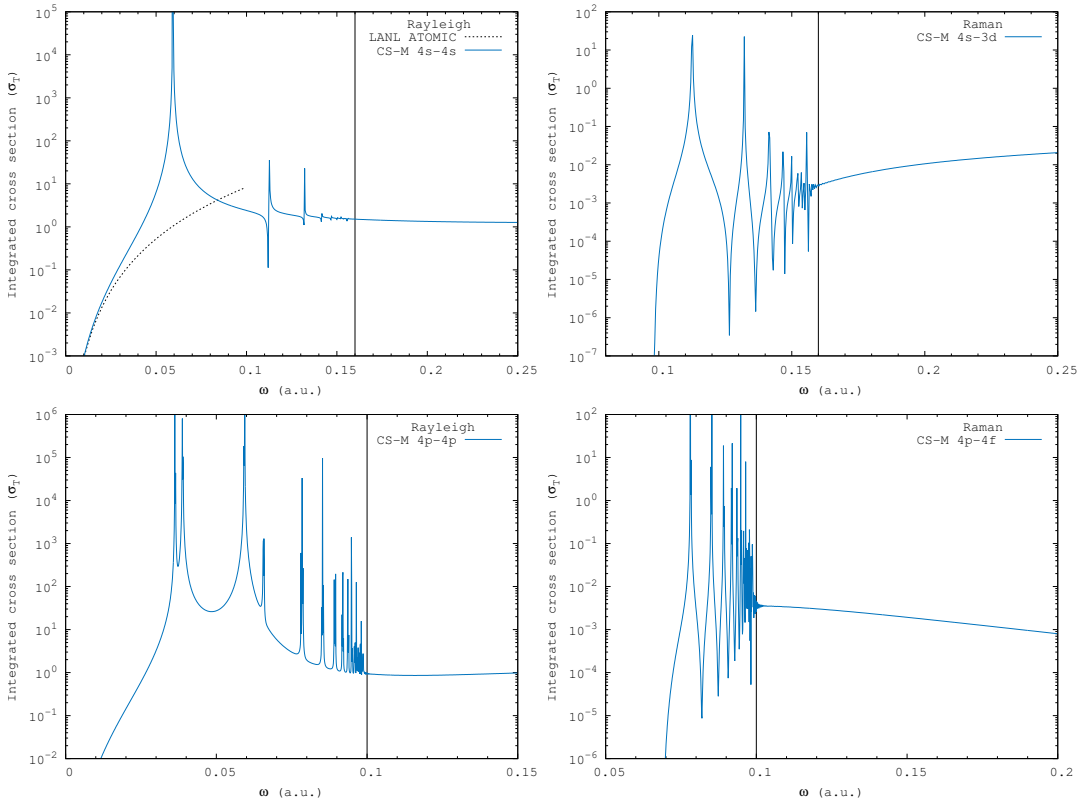

Figure 7. Same as Figure 5 but for potassium.

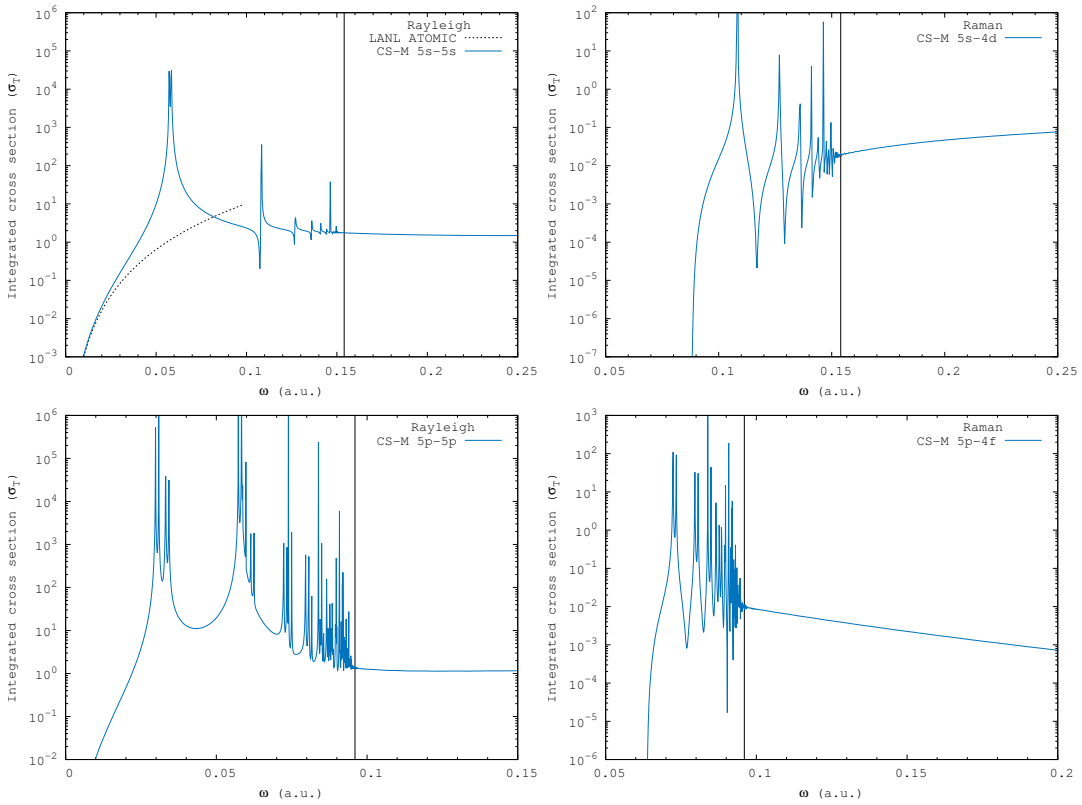

Figure 8. Same as Figure 5 but for rubidium.

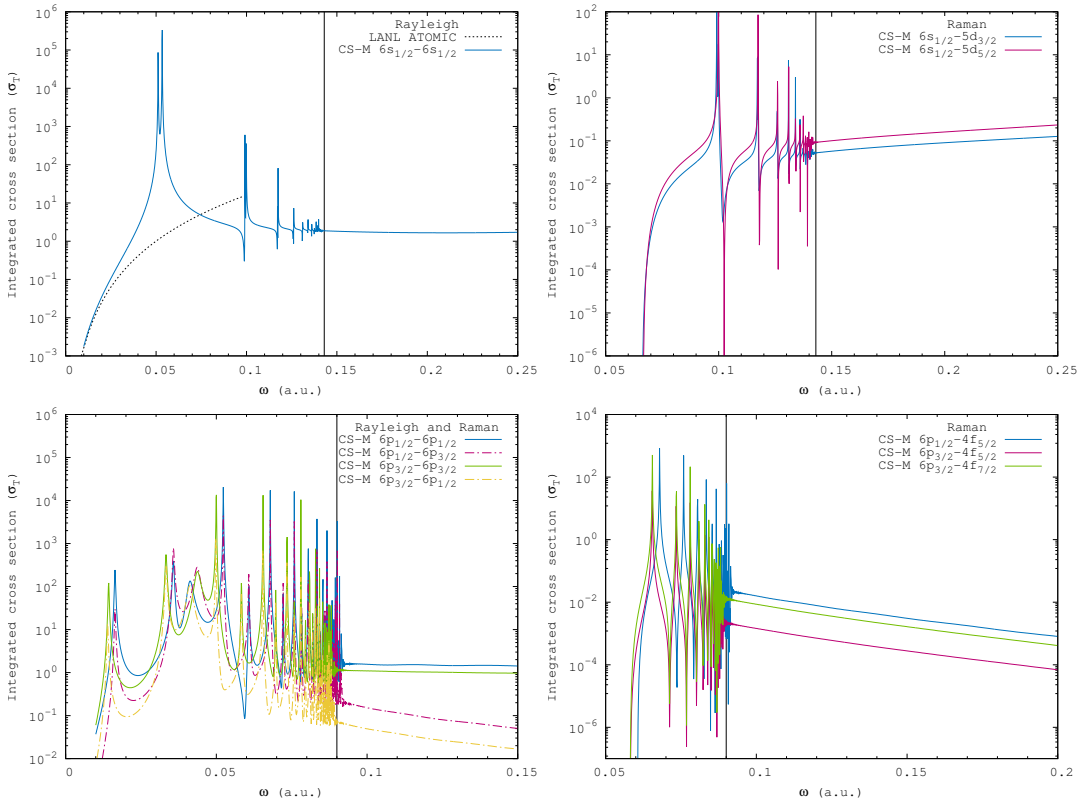

Figure 9. Same as Figure 5 but for cesium with resolved fine structure levels.

For scattering between initial and final states of the same orbital angular momentum with $l > 0$, there will be resonances for intermediate bound states with $l - 1$ and $l + 1$, which causes the larger number of resonance peaks observed in cross sections for Rayleigh scattering on the first p excited state. In Figure 9, the $6p_{1/2} \rightarrow 4f_{7/2}$ transition is not allowed by selection rules. For Rayleigh scattering on the ground state, we compared our results with the low energy approximation used in the Los Alamos National Lab ATOMIC opacity and plasma modelling code [5] and found good agreement at low energies for all alkali atoms. We have also found good agreement with the lithium and sodium ground state Rayleigh scattering cross sections of Grunefeld [15]. As discussed earlier, the convergence of the ground state Rayleigh scattering cross section is particular fast and the good agreement is expected.

Calculations of Rayleigh and Raman cross sections for scattering on alkali atoms are scarce and there are no experimental results. Apart from the results that are presented in the thesis of Grunefeld [15], we could only locate calculations due to Sadeghpour and Dalgarno [12] for cesium. In Figure 10, we compare with the results of Sadeghpour and Dalgarno [12] and find good agreement for the cesium $6s \rightarrow 6s$ Rayleigh cross section, but not for the $6s \rightarrow 7s$ Raman cross section. The cross sections of Sadeghpour and Dalgarno [12] and our CS results were calculated using the standard length form of the dipole operator. The convergence of our cross sections is rapid below the ionization threshold, only requiring the first few intermediate bound states, as we have discussed earlier. This is demonstrated explicitly in Figure 10. The origin of the discrepancy for the cesium $6s \rightarrow 7s$ Raman cross section is unclear. We note though, that we find complete agreement with all hydrogen cross sections that are presented by Sadeghpour and Dalgarno [12].

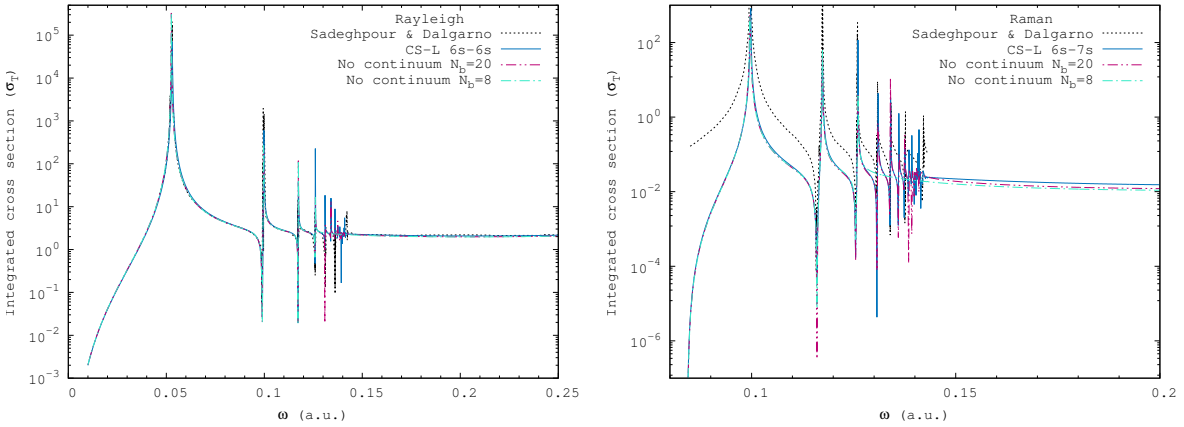

Figure 10. Length gauge cross sections for Rayleigh and Raman scattering on the ground state of cesium with comparison to the length gauge calculations of Sadeghpour and Dalgarno [12]. We demonstrate convergence of our cross sections with respect to increased number of intermediate bound states and account of continuum. N_b denotes the total number of bound intermediate states.

5. Conclusions

We have extended two computational methods for calculating cross sections for photon scattering processes on hydrogen to qausi one-electron systems. The more computationally efficient complex scaling (CS) method was used in order to calculate Rayleigh and Raman cross sections for a large number of transitions in alkali atoms from lithium to cesium. The principal value (PV) method was used as an independent check on the cross sections calculated using the CS method.

The rapid convergence of Rayleigh and Raman cross sections was observed for photon energies that were below the ionization threshold with just a few low lying bound intermediate terms required. Above the ionization threshold, we found that the account of target continuum becomes progressively more important for transitions from and to excited states. The ground state Rayleigh scattering cross sections are generally less affected by accounting for intermediate continuum states. We find that

relativistic effects are only significant for the calculation of Rayleigh and Raman scattering cross sections for heavier atoms (cesium and rubidium) where the fine structure splitting is substantial and leads to the corresponding splitting of cross section resonance peaks.

Both PV and CS methods can be generalised to the fully relativistic case, with existing techniques for calculating bound and continuum states of the Dirac–Coulomb Hamiltonian being directly applicable to the PV method. The CS method has been previously used to study resonances in Dirac Hamiltonians [35,36] demonstrating its compatibility with relativistic theory. Fully relativistic CS method calculations could be performed by utilising Dirac *L*-spinors, as done in the relativistic formulation of the convergent close-coupling method [37]. These will be pursued in future work. Relativistic effects have been found to be significant for calculating photoionization cross sections, which will be presented in a forthcoming paper.

Author Contributions: Conceptualization, A.S., D.F., K.M. and I.B.; methodology, D.F. and K.M.; software, A.S. and K.M.; validation, A.S., D.F. and K.M.; formal analysis, A.S.; investigation, A.S.; resources, D.F. and I.B.; data curation, A.S.; writing—original draft preparation, A.S.; writing—review and editing, A.S., D.F., K.M. and I.B.; visualization, A.S.; supervision, D.F.; project administration, D.F. and I.B.; funding acquisition, D.F. and I.B. All authors have read and agreed to the published version of the manuscript.

Funding: This research was funded by the the United States Air Force Office of Scientific Research, grant number FA2386-19-1-4044.

Acknowledgments: This work was supported by the Australian Research Council and resources provided by the Pawsey Supercomputing Centre, with funding from the Australian Government and Government of Western Australia.

Conflicts of Interest: The authors declare no conflict of interest.

Abbreviations

The following abbreviations are used in this manuscript:

KHW	Kramers-Heisenberg-Waller
PV	Principal value
CS	Complex scaling
LANL	Los Alamos National Lab

References

1. Kramers, H.A.; Heisenberg, W. Über die Streuung von Strahlung durch Atome. *Z. Phys.* **1925**, *31*, 681–708. [CrossRef]
2. Waller, I. Die Streuung kurzwelliger Strahlung durch Atome nach der Diracschen Strahlungstheorie. *Z. Phys.* **1929**, *58*, 75–94. [CrossRef]
3. Sampson, D.H. The Opacity at High Temperatures due to Compton Scattering. *Astrophys. J.* **1959**, *129*, 734. [CrossRef]
4. Huebner, W.F.; Barfield, W.D. *Opacity*; Springer: New York, NY, USA, 2014.
5. Colgan, J.; Kilcrease, D.P.; Magee, N.H.; Sherrill, M.E.; Abdallah, J., Jr.; Hakel, P.; Fontes, C.J.; Guzik, J.A.; Mussack, K.A. A new generation of los alamos opacity tables. *Astrophys. J.* **2016**, *817*, 116. [CrossRef]
6. Ferraro, J.H.; Nakamoto, K.; Brown, C.W. *Introductory Raman Spectroscopy*; Academic Press: San Diego, USA, 2003.
7. Lloyd, S. Enhanced Sensitivity of Photodetection via Quantum Illumination. *Science* **2008**, *321*, 1463–1465. [CrossRef]
8. Lanzagota, M. *Quantum Radar*; Morgan & Claypool: San Rafael, CA, USA, 2012.
9. Gavrila, M. Elastic Scattering of Photons by a Hydrogen Atom. *Phys. Rev.* **1967**, *163*, 147–155. [CrossRef]
10. Saslow, W.M.; Mills, D.L. Raman Scattering by Hydrogenic Systems. *Phys. Rev.* **1969**, *187*, 1025–1034. [CrossRef]
11. Dalgarno, A.; Lewis, J.T. The Exact Calculation of Long-Range Forces between Atoms by Perturbation Theory. *Proc. R. Soc. Lond. Ser.* **1955**, *233*, 70–74. [CrossRef]

12. Sadeghpour, H.R.; Dalgarno, A. Rayleigh and Raman scattering by hydrogen and caesium. *J. Phys. At. Mol. Opt. Phys.* **1992**, *25*, 4801–4809. [CrossRef]
13. Delserieys, A.; Khattak, F.Y.; Sahoo, S.; Gribakin, G.F.; Lewis, C.L.S.; Riley, D. Raman satellites in optical scattering from a laser-ablated Mg plume. *Phys. Rev. A* **2008**, *78*, 055404. [CrossRef]
14. Drühl, K. Cross section and hyperfine structure of the atomic iodine ($^2P_{\frac{1}{2}} - ^2P_{\frac{3}{2}}$) Raman transition. *Phys. Rev. A* **1982**, *26*, 863–868. [CrossRef]
15. Grunefeld, S.J. A Pseudostate Method for Computing Photon-Atom Scattering Cross-Sections. Ph.D. Thesis, The University of Queensland, Brisbane, QLD, Australia, 2017.
16. McNamara, K.; Fursa, D.V.; Bray, I. Efficient calculation of Rayleigh and Raman scattering. *Phys. Rev. A* **2018**, *98*, 043435. [CrossRef]
17. Balslev, E.; Combes, J.M. Spectral properties of many-body Schrödinger operators with dilatation-analytic interactions. *Commun. Math. Phys.* **1971**, *22*, 280–294. [CrossRef]
18. Simon, B. Quadratic form techniques and the Balslev-Combes theorem. *Commun. Math. Phys.* **1972**, *27*, 1–9. [CrossRef]
19. Rescigno, T.N.; McKoy, V. Rigorous method for computing photoabsorption cross sections from a basis-set expansion. *Phys. Rev. A* **1975**, *12*, 522–525. [CrossRef]
20. Sakurai, J. *Advanced Quantum Mechanics*; Addison-Wesley: Reading, MA, USA, 1967.
21. Landau, L.D.; Lifshitz, E.M. *Relativistic Quantum Theory*; Course of Theoretical Physics; Pergamon Press: London, UK, 1965.
22. Clementi, E.; Roetti, C. Roothaan-Hartree-Fock atomic wavefunctions: Basis functions and their coefficients for ground and certain excited states of neutral and ionized atoms, $Z \leq 54$. *At. Data Nucl. Data Tables* **1974**, *14*, 177–478. [CrossRef]
23. McLean, A.; McLean, R. Roothaan-Hartree-Fock atomic wave functions Slater basis-set expansions for Z = 55–92. *At. Data Nucl. Data Tables* **1981**, *26*, 197–381. [CrossRef]
24. Furness, J.B.; McCarthy, I.E. Semiphenomenological optical model for electron scattering on atoms. *J. Phys. At. Mol. Phys.* **1973**, *6*, 2280–2291. [CrossRef]
25. Albright, B.J.; Bartschat, K.; Flicek, P.R. Core potentials for quasi-one-electron systems. *J. Phys. At. Mol. Opt. Phys.* **1993**, *26*, 337–344. [CrossRef]
26. Norcross, D.W. Application of Scattering Theory to the Calculation of Alkali Negative-Ion Bound States. *Phys. Rev. Lett.* **1974**, *32*, 192–195. [CrossRef]
27. Mitroy, J.; Griffin, D.C.; Norcross, D.W.; Pindzola, M.S. Electron-impact excitation of the resonance transition in Ca^+. *Phys. Rev. A* **1988**, *38*, 3339–3350. [CrossRef] [PubMed]
28. Hameed, S.; Herzenberg, A.; James, M.G. Core polarization corrections to oscillator strengths in the alkali atoms. *J. Phys. At. Mol. Phys.* **1968**, *1*, 822–830. [CrossRef]
29. Lim, I.S.; Laerdahl, J.K.; Schwerdtfeger, P. Fully relativistic coupled-cluster static dipole polarizabilities of the positively charged alkali ions from Li+ to 119+. *J. Chem. Phys.* **2002**, *116*, 172–178. [CrossRef]
30. Bray, I.; Bartschat, K.; Stelbovics, A.T. Box-based convergent close-coupling method for solving Coulomb few-body problems. *Phys. Rev. A* **2003**, *67*, 060704. [CrossRef]
31. Bray, I.; Stelbovics, A.T. Convergent close-coupling calculations of electron-hydrogen scattering. *Phys. Rev. A* **1992**, *46*, 6995–7011. [CrossRef] [PubMed]
32. Bray, I.; Fursa, D.V.; Kheifets, A.S.; Stelbovics, A.T. Electrons and photons colliding with atoms: Development and application of the convergent close-coupling method. *J. Phys. At. Mol. Opt. Phys.* **2002**, *35*, R117–R146. [CrossRef]
33. Zammit, M.C.; Fursa, D.V.; Savage, J.S.; Bray, I. Electron- and positron-molecule scattering: Development of the molecular convergent close-coupling method. *J. Phys. At. Mol. Opt. Phys.* **2017**, *50*, 123001. [CrossRef]
34. Moiseyev, N.; Certain, P.; Weinhold, F. Resonance properties of complex-rotated hamiltonians. *Mol. Phys.* **1978**, *36*, 1613–1630. [CrossRef]
35. Alhaidari, A.D. Relativistic extension of the complex scaling method. *Phys. Rev. A* **2007**, *75*, 042707. [CrossRef]
36. Šeba, P. The complex scaling method for Dirac resonances. *Lett. Math. Phys.* **1988**, *16*, 51–59. [CrossRef]
37. Fursa, D.V.; Bray, I. Fully Relativistic Convergent Close-Coupling Method for Excitation and Ionization Processes in Electron Collisions with Atoms and Ions. *Phys. Rev. Lett.* **2008**, *100*, 113201. [CrossRef] [PubMed]